Title	Systematic study of electronic and magnetic properties for Cu_<12-x> TM_xSb_4S_<13> (TM= Mn, Fe, Co, Ni, and Zn) tetrahedrite
Author(s)	Suekuni, K.; Tomizawa, Y.; Ozaki, T.; Koyano, M.
Citation	Journal of Applied Physics, 115(14): 143702-1-143702-5
Issue Date	2014-04-09
Type	Journal Article
Text version	publisher
URL	http://hdl.handle.net/10119/12894
Rights	Copyright 2014 American Institute of Physics. This article may be downloaded for personal use only. Any other use requires prior permission of the author and the American Institute of Physics. The following article appeared in K. Suekuni, Y. Tomizawa, T. Ozaki, and M. Koyano, Journal of Applied Physics, 115(14), 143702 (2014) and may be found at http://dx.doi.org/10.1063/1.4871265
Description	

K. Suekuni, Y. Tomizawa, T. Ozaki, and M. Koyano

Articles you may be interested in

Magnetism and superconductivity in MxFe1+yTe1–zSez (M=Cr, Mn, Co, Ni, Cu, and Zn) single crystals
J. Appl. Phys. **109**, 07E113 (2011); 10.1063/1.3565424

Room-temperature spin glass and near band edge properties of highly disorder (FeCo) 0.03 Zn 0.97 O and (FeCoNi) 0.03 Zn 0.97 O nanorods
J. Appl. Phys. **107**, 043902 (2010); 10.1063/1.3284076

Theoretical investigation of half metallicity in Fe/Co/Ni doped ZnSe material systems
J. Appl. Phys. **106**, 093710 (2009); 10.1063/1.3256186

Temperature dependence of solubility limits of transition metals (Co, Mn, Fe, and Ni) in ZnO nanoparticles
Appl. Phys. Lett. **89**, 144105 (2006); 10.1063/1.2360176

Correlation of magnetic property with electrical transport property for ferromagnetic (Zn 1 − x Mn x) O thin films
J. Appl. Phys. **98**, 123905 (2005); 10.1063/1.2147845
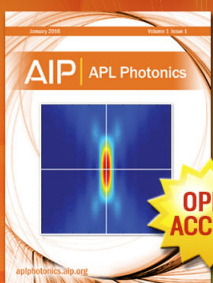
Systematic study of electronic and magnetic properties for $Cu_{12-x}TM_xSb_4S_{13}$ (TM = Mn, Fe, Co, Ni, and Zn) tetrahedrite

K. Suekuni,[1,a)] Y. Tomizawa,[2] T. Ozaki,[2,3] and M. Koyano[2,4]

[1]*Department of Quantum Matter, ADSM, Hiroshima University, Higashi-Hiroshima 739-8530, Japan*
[2]*School of Materials Science, Japan Advanced Institute of Science and Technology, 1-1 Asahidai, Nomi, Ishikawa 923-1292, Japan*
[3]*Research Center for Simulation Science, Japan Advanced Institute of Science and Technology, 1-1 Asahidai, Nomi, Ishikawa 923-1292, Japan*
[4]*Green Devices Research Center, Japan Advanced Institute of Science and Technology, 1-1 Asahidai, Nomi, Ishikawa 923-1292, Japan*

Substitution effects of 3d transition metal (TM) impurities on electronic and magnetic properties for $Cu_{12}Sb_4S_{13}$ tetrahedrite are investigated by the combination of low-temperature experiments and first-principles electronic-structure calculations. The electrical resistivity for the cubic phase of $Cu_{12}Sb_4S_{13}$ exhibits metallic behavior due to an electron-deficient character of the compound. Whereas that for $0.5 \leq x \leq 2.0$ of $Cu_{12-x}Ni_xSb_4S_{13}$ exhibits semiconducting behavior. The substituted Ni for Cu is in the divalent ionic state with a spin magnetic moment and creates impurity bands just above the Fermi level at the top of the valence band. Therefore, the semiconducting behavior of the electrical resistivity is attributed to the thermal excitation of electrons from the valence band to the impurity band. The substitution effect of TM on the electronic structure and the valency of TM for $Cu_{11.0}TM_{1.0}Sb_4S_{13}$ are systematically studied by the calculation. The substituted Mn, Fe, and Co for Cu are found to be in the ionic states with the spin magnetic moments due to the large exchange splitting of the 3d bands between the minority- and majority-spin states. © 2014 AIP Publishing LLC. [http://dx.doi.org/10.1063/1.4871265]

I. INTRODUCTION

Substituted or doped 3d transition metal (TM) elements in binary compound semiconductors are known as deep-level impurities, which strongly modify the electronic structure.[1–4] Valence states and d-band structures for the TM impurities have attracted as much interest from their technological importance as well as from the viewpoint of basic physics. Particularly, diluted ferromagnetic semiconductors such as $In_{1-x}Mn_xAs$,[5–8] $Ga_{1-x}Mn_xAs$,[9,10] and $Zn_{1-x}Cr_xTe$[11,12] are expected to be used in spintronics devices. Compared to the binary compound semiconductors with the zinc blende structure,[5–12] the substitution effect of the TM impurities on the electronic structure for ternary/electron-deficient semiconductors has been scarcely studied.

$Cu_{12}Sb_4S_{13}$ tetrahedrite is an electron-deficient semiconductor which has a band gap of 1.2–1.7 eV between the valence band (VB) and the conduction band (CB) and has two unoccupied states in the VB.[13–16] The compound is known as a mother phase of high-performance and environmentally friendly thermoelectric materials $Cu_{12-x}TM_xSb_4S_{13}$ (TM = Fe, Ni, and Zn)[15,17–20] and as a candidate for application in photovoltaic devices as well as in strong near infrared absorbers.[16] $Cu_{12}Sb_4S_{13}$ has the cubic crystal structure ($I\bar{4}3m$) at room temperature.[18,21–24] The structure is constructed by independent two Cu, two S, and one Sb crystallographic sites. Cu(1) occupies a tetrahedral void of S atoms and Cu(2) locates in a sulfur triangle, as shown in Fig. 1.

We have reported the low-temperature electrical resistivity ρ for $Cu_{12}Sb_4S_{13}$ and $Cu_{10}TM_2Sb_4S_{13}$ (TM = Mn, Fe, Co, Ni, and Zn).[17] $Cu_{12}Sb_4S_{13}$ exhibits a metal-semiconductor transition (MST) at 85 K with decreasing temperatures. On the other hand, $\rho(T)$ for $Cu_{10}TM_2Sb_4S_{13}$ exhibits the semiconducting behavior without the MST in the whole temperature range. For TM = Zn, the substituted Zn for Cu supplies the electron to the VB, and then the VB is filled, so that the semiconducting behavior of $\rho(T)$ exhibits.[15] For TM = Ni, it is expected that the substituted Ni for Cu supplies the hole to the VB and that the metallic behavior of $\rho(T)$ appears like in the cubic phase of $Cu_{12}Sb_4S_{13}$. Contrary to the expectations, $\rho(T)$ for TM = Ni exhibits semiconducting behavior.

In the present work, we studied TM substitution effects on the electronic and magnetic properties for $Cu_{12}Sb_4S_{13}$ by the combination of low-temperature experiments and first-principles electronic-structure calculations. For $Cu_{12-x}Ni_xSb_4S_{13}$, we performed low-temperature ρ and magnetic susceptibility χ measurements on polycrystalline samples of $x = 0$, 0.5, 1.0, 1.5, and 2.0 and the calculations on $x = 0$, 1.0, and 2.0. Furthermore, the electronic structure and the valence state of the TM impurity for $Cu_{11.0}TM_{1.0}Sb_4S_{13}$ (TM = Mn, Fe, Co, and Zn) were studied systematically by the calculation.

II. EXPERIMENTAL DETAILS AND CALCULATION METHOD

The sample of $Cu_{12-x}Ni_xSb_4S_{13}$ ($x = 0$, 0.5, 1.0, 1.5, and 2.0) with a relative density higher than 96% has been prepared by the hot-press method as described previously.[18] Temperature dependence of ρ was measured in a physical
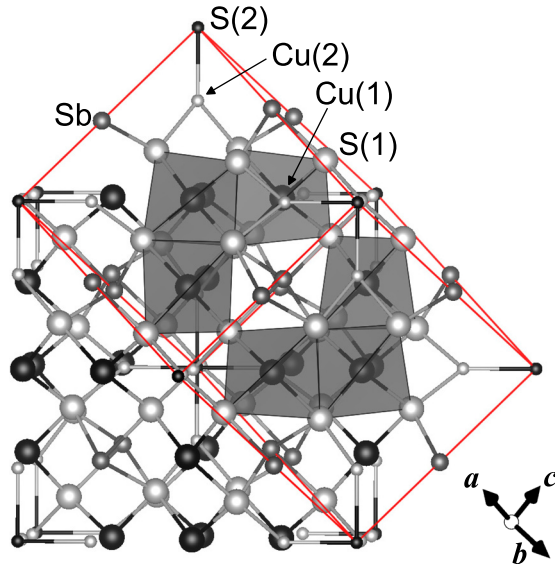
a)ksuekuni@hiroshima-u.ac.jp

FIG. 1. Bcc cubic structure ($I\bar{4}3m$) and primitive cell of $Cu_{12}Sb_4S_{13}$ tetrahedrite. Edge of the primitive cell is depicted by solid lines. CuS_4 tetrahedra are shaded.

property measurement system (PPMS, Quantum Design) using an ac four probe method at temperatures between 3 K and 340 K. For the measurement, Au-wire electrodes were attached to the sample surface using a gold paste. Temperature dependence of M was measured using a superconducting quantum interference device (SQUID) magnetometer on a magnetic property measurement system (MPMS, Quantum Design) at temperatures between 2 K and 340 K under a constant magnetic field B of 10 kOe.

The electronic structure of $Cu_{12-x}Ni_xSb_4S_{13}$ ($x = 0$, 1.0, and 2.0) and $Cu_{11.0}TM_{1.0}Sb_4S_{13}$ (TM = Mn, Fe, Co, and Zn) was calculated with the OpenMX software package[25] based on density functional theories (DFT), norm-conserving pseudopotentials, and pseudo-atomic localized basis functions. The electronic structure was self-consistently determined under an electronic temperature of 300 K by means of the spin polarized DFT within the generalized gradient approximation proposed by Perdew, Burke, and Ernzerhof.[26] We used pseudo-atomic orbitals basis functions of Cu8.0-s3p3d2, TM8.0-s3p3d2, Sb7.0-s3p3d3f1, and S7.0-s3p3d2f1, where the first symbol denotes the chemical name, followed by the cutoff radius (Bohr), and the last set of symbols denotes specification of optimized orbitals.[27] We adopted an energy cutoff of ~540 Ry in the numerical integrations and a k-point grid of $7 \times 7 \times 7$. The internal atomic coordinates and the lattice parameter were fully optimized until the maximum force becomes less than 0.0006 Hartree/Bohr for $x = 1.0$ and 2.0 of $Cu_{12-x}Ni_xSb_4S_{13}$ and less than 0.0001 Hartree/Bohr for $x = 0$ of $Cu_{12-x}Ni_xSb_4S_{13}$ and $Cu_{11.0}TM_{1.0}Sb_4S_{13}$ (TM = Mn, Fe, Co, Zn), while the unit cell was assumed to be cubic (Fig. 1). The electronic band dispersion and density of states (DOS) were calculated by using the optimized atomic coordinates and an equilibrium lattice parameter (ELP). The calculation with Hubbard U parameters of 2 eV and 4 eV for electrons in Cu-d and Ni-d orbitals was performed on the optimized structure for $U = 0$ of $Cu_{12-x}Ni_xSb_4S_{13}$.

III. RESULTS AND DISCUSSION

A. Electronic and magnetic properties for $Cu_{12-x}Ni_xSb_4S_{13}$ ($0 \leq x \leq 2.0$)

Temperature dependence of ρ for $Cu_{12-x}Ni_xSb_4S_{13}$ ($0 \leq x \leq 2.0$) is shown in Fig. 2(a). For $x = 0$, the value of ρ varies weakly with temperatures down to 275 K, increases slightly at around 225 K, jumps at around the MST temperature $T_{MST} \sim 85$ K (inset of Fig. 2(a)), and increases exponentially with decreasing temperatures. There are thermal hystereses in two regions; at around 225 K and around T_{MST}. The former hysteresis for the present sample of the density of 98% is smaller than that for a sample of the density of 80%.[17] The latter one due to the MST is similar to that for the lower-density sample.

For $x \geq 0.5$, the value of ρ at 300 K increases as x increases and $\rho(T)$ shows semiconducting behavior without anomalies at around 225 K and T_{MST}. The former result indicates decrease of the carrier density as x increases. For $x = 2.0$, $\ln\rho$ varies linearly with $1000/T$ at $T < 100$ K, as shown in Fig. 2(b). The data between 100 K and 30 K can be reproduced by using an equation $\ln\rho = \ln\rho_0 + E_A/k_BT$ (ρ_0: pre-exponential factor, k_B: Boltzmann's constant) and the activation energy E_A of 33 meV. The gap energy $E_g = 2E_A = 66$ meV is one order of magnitude smaller than the intrinsic band gap energy of 1.2–1.7 eV.[13–16] The narrow-gap structure for $x = 2.0$ presumably results in the increase of thermopower with decreasing temperatures at $T < 100$ K.[18]
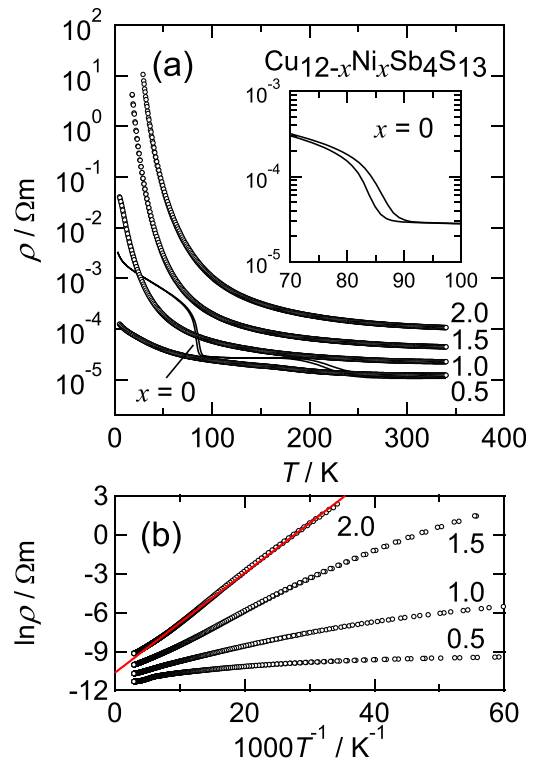

FIG. 2. (a) Temperature dependence of electrical resistivity ρ for $Cu_{12-x}Ni_xSb_4S_{13}$ ($0 \leq x \leq 2.0$). Metal-semiconductor transition at ~85 K for $x = 0$ is emphasized in the inset. The plot of $\ln\rho$ versus $1000/T$ for $x \geq 0.5$ is shown in (b). The linear line is a fit to the data (see text).
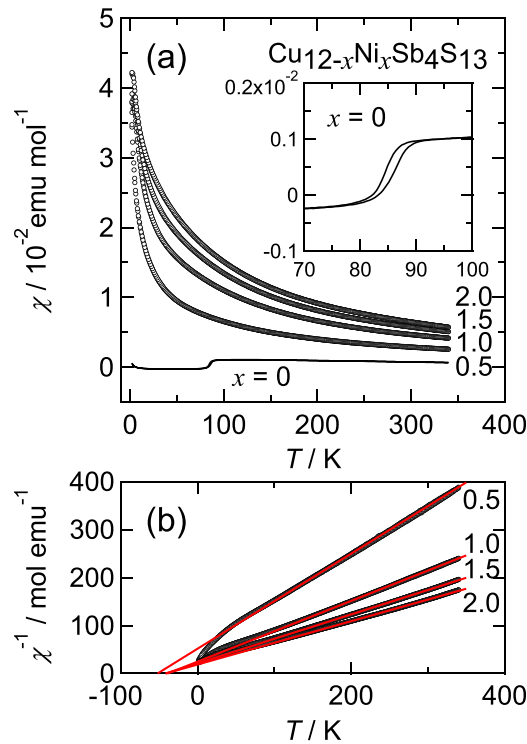
FIG. 3. (a) Temperature dependence of magnetic susceptibility $\chi = M/B$ for $Cu_{12-x}Ni_xSb_4S_{13}$ ($0 \leq x \leq 2.0$) measured in a magnetic field of 10 kOe. The transition at ~85 K for $x = 0$ is emphasized in the inset. The plot of $1/\chi$ versus T is shown in (b). The linear lines are fits to the data (see text).

Temperature dependence of $\chi = M/B$ for $Cu_{12-x}Ni_xSb_4S_{13}$ ($0 \leq x \leq 2.0$) is shown in Fig. 3(a). For $x = 0$, $\chi(T)$ exhibits the Pauli-paramagnetic behavior with a sharp drop at around T_{MST}, below which χ becomes negative, as is shown in the inset of Fig. 3(a). The thermal hysteresis is observed around T_{MST} in $\chi(T)$ as well as in $\rho(T)$. This result demonstrates that the MST is the first-order phase transition. It should be noted that χ for a sample grown in the salt KCl-LiCl flux exhibits

the positive value in the whole temperature range and $\chi(T)$ shows no hysteresis at temperatures between 79 and 86 K.[28] The disagreement in $\chi(T)$ between our and the reported samples might result from the small composition deviation.

For $x \geq 0.5$, the value of χ increases as x increases and $\chi(T)$ exhibits the Curie-Weiss behavior without the anomaly around 85 K, as shown in Fig. 3(a). The former result indicates that the substituted Ni has a magnetic moment. The inverse magnetic susceptibility $1/\chi$ for $x \geq 0.5$ is plotted in Fig. 3(b). The linear variation on T at $T > 150$ K was fitted by the Curie-Weiss law given by $1/\chi = (T - \theta)/C$, where C is the Curie constant and θ is the paramagnetic Curie temperature. The Curie constant gives the effective number of Bohr magneton p_{eff} per Ni ion which decreases from 4.0, 3.6, 3.2, to 3.0 as x increases. The value of p_{eff} for $x = 1.5$ and 2.0 is comparable to 2.83 for the spin only magnetic moment of Ni^{2+} ion with the spin S = 1. While the Ni-poor sample exhibits higher value of p_{eff}. This result might be attributed to a matter that the Pauli spin susceptibility ($\sim 10^{-3}$ emu mol^{-1} for $x = 0$ at 150 K) was not subtracted from the total χ or a matter that the substituted Ni induces the magnetic moments of Cu and S as mentioned below. The negative values of θ of -52 K for $x = 0.5$ and θ of ~ -40 K for $x \geq 1.0$ indicate that the dominant interaction between the spins of Ni is antiferromagnetic.

B. Electronic structures for $Cu_{12-x}Ni_xSb_4S_{13}$ ($0 \leq x \leq 2.0$) and $Cu_{11.0}TM_{1.0}Sb_4S_{13}$ (TM = Mn, Fe, Co, and Zn)

For $x = 0$ of $Cu_{12-x}Ni_xSb_4S_{13}$ ($Cu_{12}Sb_4S_{13}$), the atomic coordinates and the lattice parameter were optimized based on the room-temperature cubic phase, and then the ELP of 10.460 Å was obtained. The ELP is larger by 1.6% than a lattice parameter of 10.30 Å at 100 K obtained by the powder x-ray diffraction measurement. The spin-resolved electronic band dispersion and DOS are shown in Fig. 4(a). Majority-spin
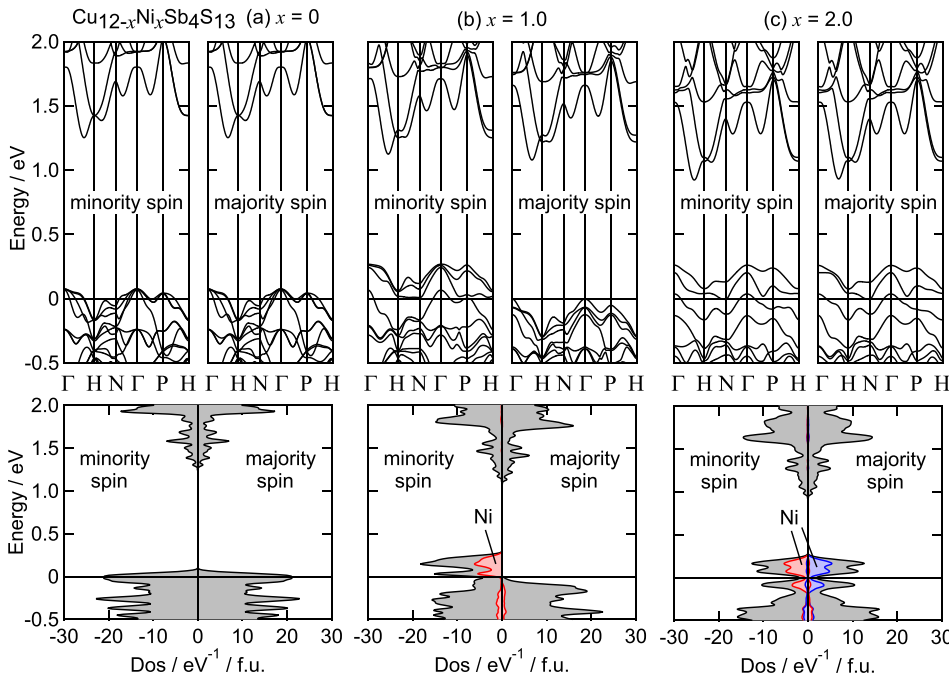

FIG. 4. Spin-resolved electronic band dispersion and DOS for $U = 0$ of $Cu_{12-x}Ni_xSb_4S_{13}$ ($x = 0$ (a), 1.0 (b), and 2.0 (c)). The red and blue areas describe partial DOS for Ni.

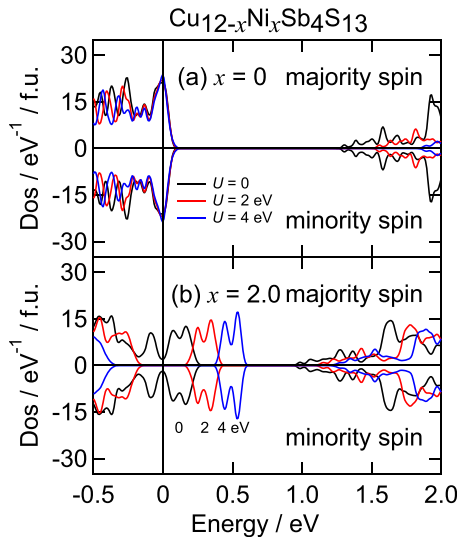FIG. 5. Spin-resolved electronic DOS for $U = 0$, 2, and 4 eV of $Cu_{12-x}Ni_xSb_4S_{13}$ ($x = 0$ (a) and 2.0 (b)).

bands agree with minority-spin ones that indicates a non-magnetic character for $x = 0$. The calculated energy gap extends from 1.2 eV to 1.7 eV with increasing the U values from 0 to 4 eV, as shown in Fig. 5(a). The gap energy for $U = 4$ eV agrees with the energy of 1.7 eV obtained by the ultraviolet photoelectron spectroscopy.[16]

The Fermi level E_F ($E = 0$ in figures) for $x = 0$ lies on the VB top with a sharp peak of the DOS, as shown in Figs. 4(a) and 5(a). There are two unoccupied states in the VB. The overall feature is consistent with that reported previously.[13–15] The electron deficient character for $x = 0$ results in the metallic behavior in $\rho(T)$ at $T > T_{MST}$. For $U = 0$, the VB in the vicinity of E_F consists mainly of hybridized orbitals of Cu-3d and S-3p. Whereas for $U = 4$ eV, the S-3p component becomes dominant. For either case, the VB top is constructed by several bands around Γ- and P-points. The bands around the P-point project upward from E_F in our result that is different from the reported electronic structure in which the bands lie at energy slightly below E_F.[15]

For $x = 1.0$, we found that the substitution of Ni for Cu(1) is 0.27 eV more stable than that for Cu(2) and the spin-polarized state is energetically favorable. The optimizations of the atomic coordinates and the lattice parameter give the ELP of 10.439 Å. For $x = 2.0$, the optimizations were

performed within a lowest-energy configuration wherein two Ni locate at the nearest-neighbor tetrahedral sites. Here, we assumed that the spin directions of two Ni are antiparallel (antiferromagnetic) based on the experimental results. As a result, we obtained the ELP of 10.420 Å.

The spin-resolved band dispersion and DOS for $U = 0$ of $x = 1.0$ and $x = 2.0$ are shown in Figs. 4(b) and 4(c), respectively. In these figures, partial DOS for Ni is also displayed. For $x = 1.0$, three minority-spin bands are lifted up above E_F in comparison with $x = 0$ and the majority-spin VB is fully occupied. The minority-spin DOS just above E_F consist mainly of the Ni-3d, Cu-3d, and S-3p orbitals. This result suggests that the substituted Ni induces the magnetic moments of Cu and S. For $x = 2.0$, two bands are lifted up above E_F in both the spin states. The lifted bands, impurity bands (IBs), consist mainly of the Ni-3d and S-3p orbitals. The Number of the IBs (2) above E_F agrees with that of the unoccupied 3d states for Ni^{2+} ($3d^8$) which was confirmed experimentally. According to the result, we will consider the number of IBs above E_F as the number of unoccupied 3d states for the TM impurity in the following discussion for $Cu_{11.0}TM_{1.0}Sb_4S_{13}$. With increasing the U values from 0 to 4 eV, the IBs move toward a deeper position of the gap between the VB and the CB, as shown in Fig. 5(b). The E_F for $U \geq 2$ eV stays in a gap between the VB and the IB that probably results in the semiconducting behavior of $\rho(T)$ for $x = 2.0$.

For $Cu_{11.0}TM_{1.0}Sb_4S_{13}$ (TM = Mn, Fe, Co, and Zn), we found that TM prefers to substitute for Cu(1) and the spin-polarized state is energetically favorable. Indeed, for TM = Fe, neutron powder diffraction[29] and Mössbauer spectroscopy[30] results have confirmed that iron is in the Cu(1) site. The TM = Mn, Fe, Co, and Zn have the ELPs of 10.497 Å, 10.468 Å, 10.448 Å, and 10.491 Å, respectively.

The spin-resolved DOS for $U = 0$ of TM = Mn, Fe, Co, and Zn is shown in Fig. 6 together with that of TM = Ni. The partial DOS for the TM impurity is also displayed in the figure. Since the decomposed DOS of the s- and p-orbitals for TM distribute well in energy whereas that of the 3d orbitals is localized, the (broad) peak structure of the partial DOS in the figure is composed of the 3d orbitals.

For TM = Mn, the DOS for the 3d orbitals lie in the minority-spin CB and the majority-spin VB, as shown in Fig. 6(a): The minority-spin 3d bands are hardly occupied, while the majority-spin ones are occupied. This result suggests that
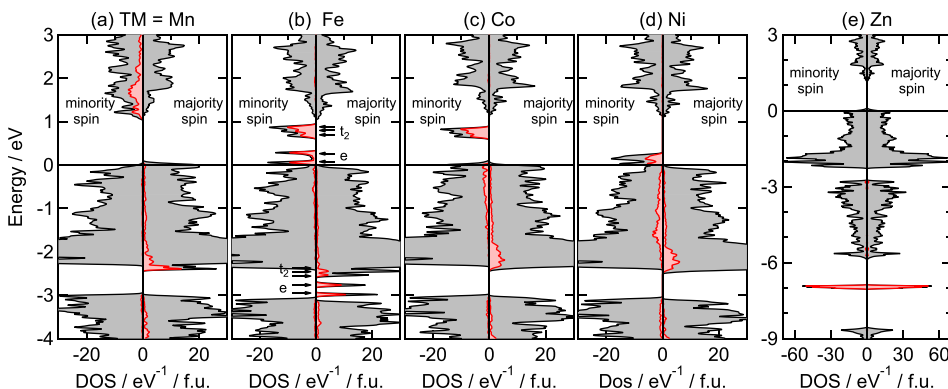

FIG. 6. Spin-resolved electronic DOS for $U = 0$ of $Cu_{11.0}TM_{1.0}Sb_4S_{13}$ (TM = Mn (a), Fe (b), Co (c), Ni (d), and Zn (e)). The red area describes partial DOS for TM.

manganese is in the Mn^{2+} ($3d^5$) high-spin configuration. For TM = Fe, the minority-spin 3d bands appear in the band gap and the majority-spin 3d bands lie in the VB at about 2.5 eV below E_F, as shown in Fig. 6(b). This result is in agreement with a result of previous calculation.[15] Five IBs consisting mainly of the Fe-3d and S-3p orbitals appear above E_F that suggests iron is in the Fe^{3+} (d^5) high-spin state. The replacement of Fe^{3+} for Cu was ascertained by the Fe Mössbauer experiment for $x = 0.5$ and 1.0 of $Cu_{12-x}Fe_xSb_4S_{13}$.[30] (For $x \geq 1.5$, substitution of Fe^{2+} for Cu takes place.) We can clearly see the crystal field splitting of the 3d bands into t_2 and e bands that is expected for iron in a tetrahedral site. For TM = Co, the minority-spin 3d bands appear in the band gap and the majority-spin 3d bands lie in the VB at about 2 eV below E_F, as shown in Fig. 6(c). Three IBs consisting mainly of the Co-3d and S-3p orbitals appear above E_F that suggests cobalt is in the Co^{2+} (d^7) state. For TM = Ni, the 3d bands appear at energy just above E_F in the minority-spin state and lie in the majority-spin VB at about 2 eV below E_F, as shown in Fig. 6(d). For TM = Zn, the 3d bands lie at 7 eV below E_F, as shown in Fig. 6(e), implying that zinc is in the Zn^{2+} (d^{10}) state. Thus, the 3d bands for TM = Mn, Fe, Co, and Ni show the exchange splitting of 2 eV–3.5 eV between the minority and majority spin states and the minority-spin 3d bands shift down in energy on going from Mn to Ni. The former character leads to the high-spin states of Mn^{2+} and Fe^{3+} ions.

In the electron-deficient semiconductor $Cu_{12}Sb_4S_{13}$, the substituted Mn, Fe, Co, and Ni for Cu(1) have spin magnetic moment like in the binary compound semiconductors.[3] For $Cu_{11.0}TM_{1.0}Sb_4S_{13}$, TM supplies electron to the VB that decrease the number of holes contributing to the electrical conduction. This feature is different from that for GaAs: the substituted Mn dopes large number of carriers which contribute to the conduction and induce the ferromagnetism.[31] Further experimental and theoretical works on $Cu_{12-x}TM_xSb_4S_{13}$ ($x > 1.0$) are required to confirm the magnetism and the types of exchange interaction between magnetic moments of the TM ions.

IV. CONCLUSION

The electronic and magnetic properties of $Cu_{12-x}Ni_xSb_4S_{13}$ ($0 \leq x \leq 2.0$) were investigated by the combination of experimental and theoretical studies. The results confirm that the substituted Ni is in the divalent ionic state with the spin magnetic moment due to the large exchange splitting of the 3d bands between the minority- and majority-spin states. The thermal excitation of electrons from the VB to the IB results in the semiconducting behavior of $\rho(T)$ for $x = 2.0$. The electronic-structure calculation for $Cu_{11.0}TM_{1.0}Sb_4S_{13}$ (TM = Mn, Fe, Co, and Ni) proposed that the TM impurity is in the divalent or trivalent ionic states and modifies electronic structure.

[1]J. K. Furdyna, J. Appl. Phys. **64**, R29 (1988).
[2]H. Ohno, J. Magn. Magn. Mater. **200**, 110 (1999).
[3]K. Sato, L. Bergqvist, J. Kudrnovský, P. H. Dederichs, O. Eriksson, I. Turek, B. Sanyal, G. Bouzerar, H. Katayama-Yoshida, V. A. Dinh, T. Fukushima, H. Kizaki, and R. Zeller, Rev. Mod. Phys. **82**, 1633 (2010).
[4]M. Tanaka, S. Ohya, and P. N. Hai, Appl. Phys. Rev. **1**, 011102 (2014).
[5]H. Munekata, H. Ohno, S. von Molnar, Armin Segmüller, L. L. Chang, and L. Esaki, Phys. Rev. Lett. **63**, 1849 (1989).
[6]H. Munekata, H. Ohno, R. R. Ruf, R. J. Gambino, and L. L. Chang, J. Cryst. Growth **111**, 1011 (1991).
[7]H. Ohno, H. Munekata, T. Penney, S. von Molnár, and L. L. Chang. Phys. Rev. Lett. **68**, 2664 (1992).
[8]K. Ando and H. Munekata, J. Magn. Magn. Mater. **272–276**, 2004 (2004).
[9]H. Ohno, A. Shen, F. Matsukura, A. Oiwa, A. Endo, S. Katsumoto, and Y. Iye, Appl. Phys. Lett. **69**, 363 (1996).
[10]K. Ando, T. Hayashi, M. Tanaka, and A. Twardowski, J. Appl. Phys. **83**, 6548 (1998).
[11]H. Saito, V. Zayets, S. Yamagata, and K. Ando, Phys. Rev. Lett. **90**, 207202 (2003).
[12]H. Saito, V. Zayets, S. Yamagata, and K. Ando, J. Appl. Phys. **93**, 6796 (2003).
[13]D. W. Bullett and W. G. Dawson, J. Phys. C: Solid State Phys. **19**, 5837 (1986).
[14]D. W. Bullett, Phys. Chem. Miner. **14**, 485 (1987).
[15]X. Lu, D. T. Morelli, Y. Xia, F. Zhou, V. Ozolins, H. Chi, X. Zhou, and C. Uher, Adv. Energy Mater. **3**, 342 (2013).
[16]J. van Embden, K. Latham, N. W. Duffy, and Y. Tachibana, J. Am. Chem. Soc. **135**, 11562 (2013).
[17]K. Suekuni, K. Tsuruta, T. Ariga, and M. Koyano, Appl. Phys. Express **5**, 051201 (2012).
[18]K. Suekuni, K. Tsuruta, M. Kunii, H. Nishiate, E. Nishibori, S. Maki, M. Ohta, A. Yamamoto, and M. Koyano, J. Appl. Phys. **113**, 043712 (2013).
[19]X. Lu and D. T. Morelli, MRS Commun. **3**, 129 (2013).
[20]X. Lu and D. T. Morelli, Phys. Chem. Chem. Phys. **15**, 5762 (2013).
[21]B. J. Wuensch, Science **141**, 804 (1963).
[22]B. J. Wuensch, Z. Kristallogr. **119**, 437 (1964).
[23]N. E. Johnson, J. R. Craig, and J. D. Rimstidt, Am. Mineral. **73**, 389 (1988).
[24]A. Pfitzner, M. Evain, and V. Petricek, Acta Crystallogr., Sect. B: Struct. Sci. **53**, 337 (1997).
[25]See http://www.openmx-square.org/ for the code, OpenMX, pseudo-atomic basis functions and pseudopotentials.
[26]J. P. Perdew, K. Burke, and M. Ernzerhof, Phys. Rev. Lett. **77**, 3865 (1996).
[27]T. Ozaki, Phys. Rev. B **67**, 155108 (2003).
[28]F. Di Benedetto, G. P. Bernardini, C. Cipriani, C. Emiliani, D. Gatteschi, and M. Romanelli, Phys. Chem. Miner. **32**, 155 (2005).
[29]J. W. Andreasen, E. Makovicky, B. Lebech, and S. K. Møller, Phys. Chem. Miner. **35**, 447 (2008).
[30]E. Makovicky, K. Forcher, W. Lottermoser, and G. Amthauer, Mineral. Petrol. **43**, 73 (1990).
[31]F. Matsukura, H. Ohno, A. Shen, and Y. Sugawara, Phys. Rev. B **57**, R2037 (1998).